Available online at www.sciencedirect.com
ScienceDirect
International Journal of Heat and Mass Transfer 51 (2008) 68–82
International Journal of HEAT and MASS TRANSFER
www.elsevier.com/locate/ijhmt

Lattice Boltzmann method applied to the solution of the energy equations of the transient conduction and radiation problems on non-uniform lattices

Bittagopal Mondal, Subhash C. Mishra *

Department of Mechanical Engineering, Indian Institute of Technology Guwahati, Guwahati 781039, India

Received 18 January 2007; received in revised form 5 April 2007
Available online 2 July 2007

Abstract

Application of the lattice Boltzmann method (LBM) to solve the energy equations of conduction–radiation problems is extended on non-uniform lattices. In the LBM on non-uniform lattices, the single relaxation time based on the minimum velocity is used. This minimum velocity corresponds to the smallest size lattice. Because information propagates with the same minimum velocity in the prescribed directions from all the lattice centers, in a given time step, they are not equidistant from the neighboring lattices. Collisions in the LBM take place at the same instant. Therefore, in the LBM on non-uniform lattices, in every time step, interpolation is required to carry the information to the neighboring lattice centers. To validate this very concept in heat transfer problems involving thermal radiation, transient conduction and radiation heat transfer problems in a 1-D planar and a 2-D rectangular geometries containing absorbing, emitting and scattering medium are considered. The finite volume method (FVM) is used to compute the radiative information. In both the geometries, results for the effects of various parameters are compared for LBM–FVM on uniform and non-uniform lattices. To establish the LBM–FVM on non-uniform lattices for the combined conduction and radiation heat transfer problems, numerical experiments were performed with different cluster values. The accurate results were found in all the cases.

1. Introduction

In the recent past, the lattice Boltzmann method (LBM) has received much attention in science and engineering as a potential computational tool for solving a large class of problems. Among many other types of problems, the LBM has been successfully used to simulate a wide range of fluid flow and heat transfer problems [1–12]. Owing to its mesocopic origin, the LBM is emerging as a versatile computational method that has many advantages. In comparison to the conventional CFD solvers like the finite difference method (FDM), the finite element method (FEM) and the finite volume method (FVM), the advantages of the LBM comprises of a clear physical meaning, a simple calculation procedure, simple and more efficient implementation for parallel computation, straightforward and efficient handling of complex geometries and boundary conditions, high computational performance with regard to stability and precision, etc. [1–20]. Further, the LBM also has a memory overhead over other methods since it deals with less number of scalars [20].

The LBM has found a wide usage in fluid flow problems [4–8] and it is also finding applications in heat transfer problems involving conduction, convection and/or radiation [2,3,6,11,14–19,21–25]. Massaioli et al. [2] and Shan [3] used the LBM to analyze the Rayleigh–Benard convection in a square cavity. Solidification of a planar medium using the LBM was analyzed by Jiaung et al. [14]. Ho et al. [15,16] solved a non-Fourier heat conduction problem in a planar medium using the LBM. Chatterjee and Chakraborty [17] used the LBM to analyze solid–liquid phase transitions in the presence of thermal diffusion.

* Corresponding author. Tel.: +91 361 2582660; fax: +91 361 2690762.
E-mail address: scm_iitg@yahoo.com (S.C. Mishra).

0017-9310/$ - see front matter © 2007 Elsevier Ltd. All rights reserved.
doi:10.1016/j.ijheatmasstransfer.2007.04.030

Nomenclature

A	area
a	anisotropy factor
b	number of discrete directions in the lattice
c_p	specific heat
C	cluster value
$\vec{e}_i$	propagation velocity in the direction i in the lattice
f_i	particle distribution function in the i direction
$f_i^{(0)}$	equilibrium particle distribution function in the i direction
G	incident radiation
I	intensity
k	thermal conductivity
M_θ	number of divisions of the polar angle θ
M_ϕ	number of divisions of the azimuthal angle ϕ
m	index for direction
N	conduction–radiation parameter, $\kappa\beta/(4\sigma T_{\text{ref}}^3)$
$\hat{n}$	outer normal
P	cell center
$\vec{q}_{\text{R}}$	radiative heat flux
$\vec{r}$	position, $r(x,y,z)$
S	source term
T	temperature
t	time
V	volume of the cell
w	weight in the LBM
X, Y, Z	length of the rectangular enclosure in x-, y- and z-directions

Greek symbols

α	thermal diffusivity
β	extinction coefficient
γ	finite-difference weighing factor
ε	emissivity
θ	polar angle
κ_{a}	absorption coefficient
ζ	non-dimensional time, $\alpha\beta^2 t$
ρ	density
σ	Stefan–Boltzmann constant($=5.670\times10^{-8}$ W/m^2 K^4)
σ_{s}	scattering coefficient
τ	relaxation time
Φ	scattering phase function
ϕ	azimuthal angle
ω	scattering albedo
Ω	direction in the FVM and rate of change of the particle distribution function f_{i} in the LBM
$\Delta\Omega$	elemental solid angle

Subscripts

E, W, N, S, F, B	east, west, north, south, front and back
b	boundary
x, y, z	x, y and z reference faces
e	exit
i	inlet
k, l	index of discrete polar and azimuthal angles, respectively
P	value at the cell centre

Superscript

m	index for direction

Application of the LBM in solving energy equations of heat transfer problems involving thermal radiation was extended by Mishra and co-workers [18,19,21–25]. Mishra and Lankadasu [18] applied the LBM to solve the energy equation of transient conduction and radiation heat transfer in a planar medium with or without heat generation. They used the discrete transfer method (DTM) to compute the radiative information. The application of the LBM to the solution of the energy equation of a conduction–radiation problem in a 2-D rectangular geometry was extended by Mishra et al. [19]. In their study, the radiative information was computed using the collapsed dimension method (CDM). Raj et al. [21] used the LBM to analyze the solidification of a semitransparent planer layer. They used the DTM to compute the radiative information. Parida et al. [22] extended the work of Raj et al. [21] by considering radiative and convective cooling along the boundaries and used the discrete ordinate method (DOM) for the radiative information. Gupta et al. [23] used a variable relaxation time LBM to solve the energy equation of a temperature dependent transient conduction and radiation heat transfer in a planer medium. They used the DOM to compute the radiative information. Mishra and Roy [24] used the LBM to solve conduction–radiation problems in 1-D and 2-D rectangular geometries and used the finite volume method (FVM) to compute the radiative information. Mondal and Mishra [25] solved the same problems as those of [24] using the LBM and the DOM. In all the previous applications of the LBM to heat transfer problems [2,3,14–19,21–25], uniform size lattices/control volumes were used in the LBM.

In CFD, non-uniform or unstructured control volumes are often required to economically capture sharp variations in the quantities like temperature, heat flux, etc. In the previous applications of the LBM to heat transfer problems [2,3,14–19,21–25], unlike its application to fluid flow problems [26–29], non-uniform or unstructured lattices/control volumes have not been tested so far. However, as proposed

in the literature [1–12], if the LBM is to qualify for a versatile CFD tool, like the FDM and the FVM of the CFD, for thermal problems involving radiation, conduction and/or convection too it should work for non-uniform or unstructured lattices/control volumes. Towards the above objective, in the present work, the LBM is used to solve the energy equations of transient conduction and radiation problems in a 1-D planar and a 2-D rectangular geometry on non-uniform lattices. Different types of lattice clustering are used to test the workability of the LBM to this class of problems. Since the FVM [24,30] is more suitable to all types of control volumes than other methods like the DTM, the DOM etc. of the radiative transfer, in the present work, we too have adopted the FVM to compute the radiative information for the energy equation. To check the performance of the LBM–FVM on non-uniform lattices/control volumes, the same problems are also solved for the uniform lattices/control volumes. Results have been compared for different values of the scattering albedo, the boundary emissivity, the conduction radiation parameter and the clustering parameter.

2. Formulation

Energy equation of a transient conduction and radiation heat transfer problem without heat generation is given by

$$\rho c_p \frac{\partial T}{\partial t} = k\nabla^2 T - \nabla \cdot \vec{q}_R, \tag{1}$$

where ρ is the density, c_p is the specific heat, k is the thermal conductivity and $\vec{q}_R$ is the radiative heat flux.

The procedure of the FVM [24,30] for radiative heat transfer is much similar to that of the FVM of the CFD, on non-uniform or unstructured lattices/control volumes, this method is more suitable than rest all other numerical radiative transfer methods such as the Monte Carlo method, the DTM, the CDM and the DOM. Since the present work deals with the solution of the energy equation (1) using the LBM on non-uniform lattices, the FVM has been used to compute the radiative information $\nabla \cdot \vec{q}_R$ in Eq. (1). The details of the methodologies of the FVM adopted in the present work for the computations of $\nabla \cdot \vec{q}_R$ can be found in Mishra and Roy [24]. In the following pages, we briefly discuss the FVM for the computation of $\nabla \cdot \vec{q}_R$ and that of the LBM to solve the energy equation (Eq. (1)).

2.1. The finite volume method (FVM)

The radiative transfer equation (RTE) in any direction $\hat{s}$ about an elemental solid angle $d\Omega$ is given by

$$\frac{dI}{ds} = -\beta I + S, \tag{2}$$

where β is the extinction coefficient and S is the source term given by

$$S = \kappa_a\left(\frac{\sigma T^4}{\pi}\right) + \frac{\sigma_s}{4\pi}\int_{\Omega'=4\pi} I(\Omega')\Phi(\Omega,\Omega')\,d\Omega', \tag{3}$$

where κ_a is the absorption coefficient, σ_s is the scattering coefficient and Φ is the scattering phase function. Resolving Eq. (1) along the Cartesian coordinate directions and integrating it over the elemental solid-angle $\Delta\Omega^m$, we get

$$\frac{\partial I^m}{\partial x}D_x^m + \frac{\partial I^m}{\partial y}D_y^m + \frac{\partial I^m}{\partial z}D_z^m = -\beta I^m \Delta\Omega^m + S^m\Delta\Omega^m. \tag{4}$$

When the surface normal $\hat{n}$ is pointing towards one of the positive coordinate directions, D_x^m, D_y^m and D_z^m are given by [24]

$$D_x^m = \cos\phi^m \sin\left(\frac{\Delta\phi^m}{2}\right)[\Delta\theta^m - \cos 2\theta^m \sin(\Delta\theta^m)] \tag{5a}$$

$$D_y^m = \sin\phi^m \sin\left(\frac{\Delta\phi^m}{2}\right)[\Delta\theta^m - \cos 2\theta^m \sin(\Delta\theta^m)] \tag{5b}$$

$$D_z^m = \sin\theta^m \cos\theta^m \sin(\Delta\theta^m)\Delta\phi^m \tag{5c}$$

For $\hat{n}$ pointing towards the negative coordinate directions, signs of D_x^m, D_y^m and D_z^m are opposite to what are obtained from Eq. (5). In Eq. (4), $\Delta\Omega^m$ is given by [24]

$$\Delta\Omega^m = 2\sin\theta^m \sin\left(\frac{\Delta\theta^m}{2}\right)\Delta\phi^m \tag{6}$$

Integrating Eq. (4) over the control volume, we get

$$\begin{aligned}&\left[I_E^m - I_W^m\right]A_{EW}D_x^m + \left[I_N^m - I_S^m\right]A_{NS}D_y^m + \left[I_F^m - I_B^m\right]A_{FB}D_z^m \\ &\quad = \left[-\beta V I_P^m + V S_P^m\right]\Delta\Omega^m,\end{aligned} \tag{7}$$

where A_{EW}, A_{NS} and A_{FB} are the areas of the x-, y- and z-faces of the 3-D control volume, respectively. In Eq. (7), I with suffixes E, W, N, S, F and B designate east, west, north, south, front and back control surface average intensities, respectively. On the right-hand side of Eq. (7), $V = dx \times dy \times dz$ is the volume of the cell and I_P^m and S_P^m are the volume averaged intensities and source term at the cell centre P, respectively.

In any discrete direction Ω^m, if a linear relationship among the two cell-surface intensities and cell-centre intensity I_P^m is assumed, then

$$\begin{aligned}I_P^m &= \gamma_x I_E^m + (1-\gamma_x)I_W^m = \gamma_y I_N^m + (1-\gamma_y)I_S^m \\ &= \gamma_z I_F^m + (1-\gamma_z)I_B^m,\end{aligned} \tag{8}$$

where γ is the finite-difference weighting factor and its value is normally considered to be 0.5. While marching from the first octant of a 3-D enclosure, for which D_x^m, D_y^m and D_z^m are all positive, I_P^m in terms of known cell-surface intensities can be written as [24]

$$I_P^m = \frac{\frac{D_x^m A_{EW}}{\gamma_x}I_W^m + \frac{D_y^m A_{NS}}{\gamma_y}I_S^m + \frac{D_z^m A_{FB}}{\gamma_z}I_B^m + V\Delta\Omega^m S_P^m}{\frac{D_x^m A_E}{\gamma_x} + \frac{D_y^m A_N}{\gamma_y} + \frac{D_y^m A_F}{\gamma_z} + \beta V\Delta\Omega^m}, \tag{9}$$

where

$$A_{\mathrm{EW}} = (1-\gamma_x)A_{\mathrm{E}} + \gamma_x A_{\mathrm{W}}, A_{\mathrm{NS}} = (1-\gamma_y)A_{\mathrm{N}} + \gamma_y A_{\mathrm{S}}, A_{\mathrm{FB}} = (1-\gamma_z)A_{\mathrm{F}} + \gamma_z A_{\mathrm{B}} \quad (10)$$

are the averaged areas. When any one of the D_x^m, D_y^m or D_z^m is negative, marching starts from other corners. In this case, a general expression of I_P^m in terms of known intensities and source term can be written as

$$I_P^m = \frac{\frac{|D_x^m|A_x}{\gamma_x} I_{x_\mathrm{i}}^m + \frac{|D_y^m|A_y}{\gamma_y} I_{y_\mathrm{i}}^m + \frac{|D_z^m|A_z}{\gamma_z} I_{z_\mathrm{i}}^m + V\Delta\Omega^m S_P^m}{\frac{|D_x^m|A_{x_\mathrm{e}}}{\gamma_x} + \frac{|D_y^m|A_{y_\mathrm{e}}}{\gamma_y} + \frac{|D_z^m|A_{z_\mathrm{e}}}{\gamma_z} + \beta V\Delta\Omega^m}, \quad (11)$$

where in Eq. (11), x_i, y_i and z_i suffixes over I^m are for the intensities entering the control volume through x-, y- and z-faces, respectively and A_x, A_y and A_z are given by

$$A_x = (1-\gamma_x)A_{x_\mathrm{e}} + \gamma_x A_{x_\mathrm{i}}, \quad A_y = (1-\gamma_y)A_{y_\mathrm{e}} + \gamma_y A_{y_\mathrm{i}}, \quad A_z = (1-\gamma_z)A_{z_\mathrm{e}} + \gamma_z A_{z_\mathrm{i}}. \quad (12)$$

In Eq. (11) A with suffixes x_i, y_i and z_i represent control surface areas through which intensities enter the control volume, while A with suffixes x_e, y_e and z_e represent control surface areas through which intensities leave the control volume.

For a linear anisotropic phase function $\Phi(\Omega,\Omega') = 1 + a\cos\theta\cos\theta'$, the source term S at any location $\vec{r}$ is in terms of the incident radiation G and net radiative heat flux q_R is written as

$$S = \frac{\sigma_\mathrm{s}}{4\pi}[G + a\cos\theta q_\mathrm{R}]. \quad (13)$$

In Eq. (13), G and q_R are numerically computed from the following [24]

$$G \approx \sum_{k=1}^{M_\phi}\sum_{l=1}^{M_\theta} I^m(\theta_l^m,\phi_k^m)2\sin\theta_l^m \sin\left(\frac{\Delta\theta_l^m}{2}\right)\Delta\phi_k^m \quad (14)$$

$$q_\mathrm{R} \approx \sum_{k=1}^{M_\phi}\sum_{l=1}^{M_\theta} I^m(\theta_l^m,\phi_k^m)\sin\theta_l^m\cos\theta_l^m\sin(\Delta\theta_l^m)\Delta\phi_k^m, \quad (15)$$

where M_θ and M_ϕ are the number of discrete points considered over the complete span of the polar angle ($0 \leqslant \theta \leqslant \pi$)and azimuthal angle ($0 \leqslant \phi \leqslant 2\pi$), respectively. For a diffuse-gray boundary having temperature T_b and emissivity ε_b, the boundary intensity I_b is computed from

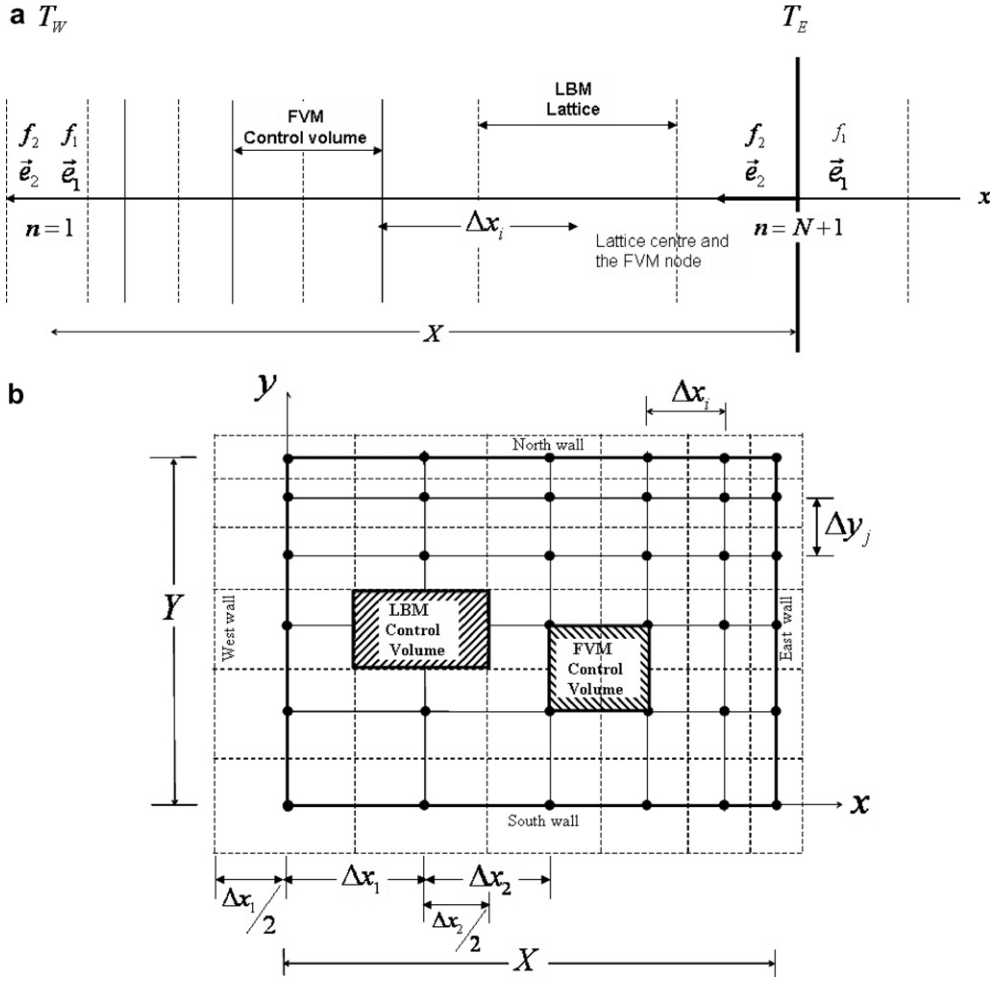

Fig. 1. Geometry and arrangements of the lattices of the LBM and control volumes of the FVM for calculation of radiative information with non-uniform lattices/control volumes (a) 1-D planar medium and (b) 2-D rectangular geometry.

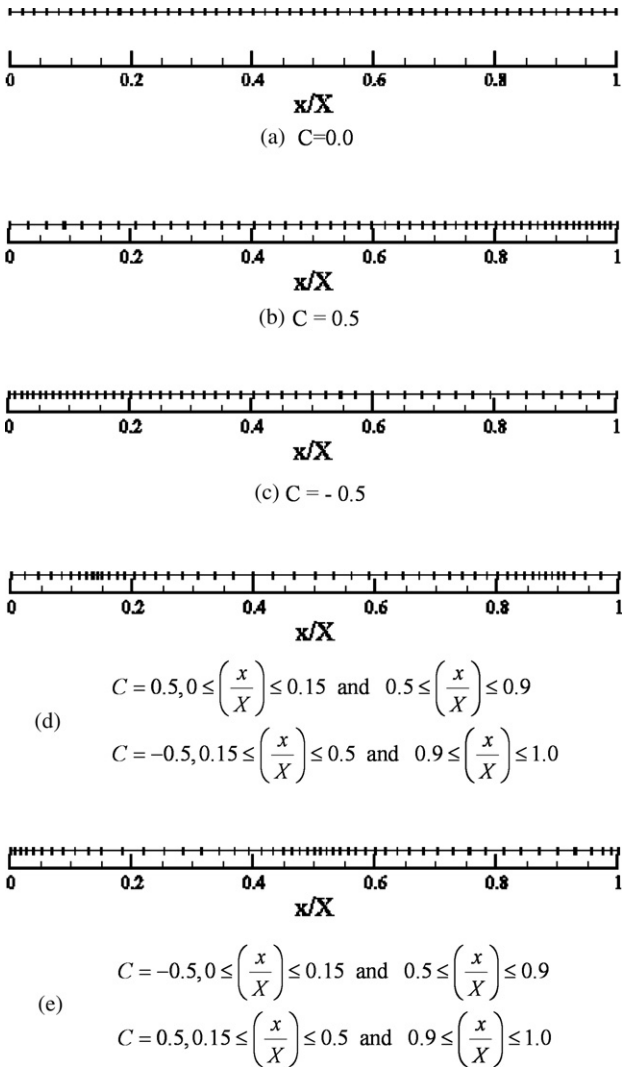

Fig. 2. Different types of non-uniform lattices for the 1-D planar medium.

$$I_b = \frac{\varepsilon_b \sigma T_b^4}{\pi} + \left(\frac{1-\varepsilon_b}{\pi}\right) \sum_{k=1}^{M_\phi} \sum_{l=1}^{M_\theta/2} I^m(\theta_l^m, \phi_k^m) \sin\theta_l^m \times \cos\theta_l^m \sin\Delta\theta_l^m \Delta\phi_k^m. \quad (16)$$

Once the intensity distributions are known, radiative information $\nabla \cdot \vec{q}_R$ required for the energy equation is computed from

$$\nabla \cdot \vec{q}_R = \beta(1-\omega)\left(4\pi\frac{\sigma T^4}{\pi} - G\right), \quad (17)$$

where in Eq. (17), $\omega = \sigma_s/\beta$ is the scattering albedo.

2.2. Lattice Boltzmann method (LBM) formulation

For the sake of completeness and also to describe the implementation of the LBM on non-uniform lattices for solving energy equations of a transient conduction–radiation problem, we briefly provide here the formulation of the LBM. Details on the implementation of the LBM to heat transfer problems involving thermal radiation can be found in the works of Mishra and co-workers [18,19,21–25].

The discrete Boltzmann equation that describes the evolution of the particle distribution function f_i is written as [9,10]

$$f_i(\vec{r} + \vec{e}_i\Delta t, t + \Delta t) = f_i(\vec{r}, t) - \frac{\Delta t}{\tau}[f_i(\vec{r}, t) - f_i^{(0)}(\vec{r}, t)], \quad i = 1, 2, 3, \ldots, b, \quad (18)$$

where f_i is the particle distribution function, $\vec{e}_i$ is the velocity, τ is the relaxation time, $f_i^{(0)}$ is the equilibrium distribution function and b is the number of directions in a lattice through which the information propagates. In heat transfer problems, τ for the D1Q2 and D2Q9 lattices are computed respectively as

$$\text{D1Q2} \quad \tau = \frac{\alpha}{|\vec{e}_i|^2} + \frac{\Delta t}{2}, \quad (19)$$

$$\text{D2Q9} \quad \tau = \frac{3\alpha}{|\vec{e}_i|^2} + \frac{\Delta t}{2}, \quad (20)$$

with f_i known, the temperature T is obtained from the following:

$$T(\vec{r}, t) = \sum_{i=0}^{b} f_i(\vec{r}, t). \quad (21)$$

To process Eq. (18), an equilibrium distribution function is required which is given by

$$f_i^{(0)}(\vec{r}, t) = w_i T(\vec{r}, t), \quad (22)$$

where w_i is the weight corresponding to the i direction and for different lattices its values are given in [24]. From Eqs. (21) and (22), we also have

Table 1
Comparison of transient temperature θ at time $\zeta = 0.05$ for $\beta = 1.0$, $T_E = 0.0$, $\omega = 0.5$, and $N = 0.1$ and two sets of wall reflectivities

ε_W	ε_E	Investigators	Transient temperature $\frac{T}{T_W}$		
			$x/X = 0.25$	$x/X = 0.50$	$x/X = 0.75$
1.0	1.0	Barker and Sutton [31]	0.4893	0.1775	0.0588
		Sutton [32]	0.4888	0.1778	0.0591
		Tsai and Lin [33]	0.4889	0.1773	0.0588
		Talukdar and Mishra [34]	0.4892	0.1768	0.0585
		Uniform lattices (present)	0.4898	0.1771	0.0581
		Non-uniform lattices (present)	0.4898	0.1771	0.0581
1.0	0.0	Barker and Sutton [31]	0.5035	0.2003	0.0831
		Sutton [32]	0.5030	0.2005	0.0833
		Tsai and Lin [33]	0.5031	0.2001	0.0830
		Talukdar and Mishra [34]	0.5033	0.1995	0.0824
		Uniform lattices (present)	0.5018	0.1965	0.0817
		Non-uniform lattices (present)	0.5010	0.1953	0.0804

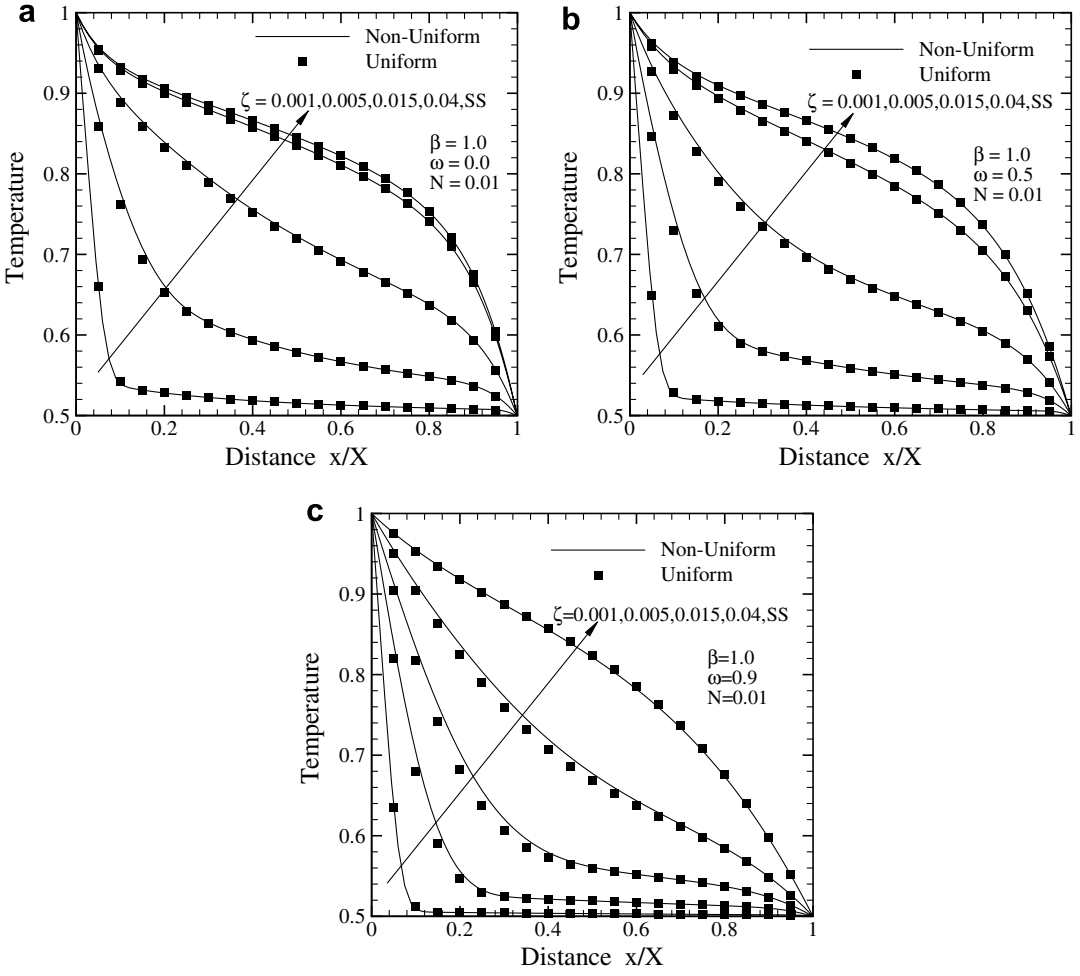

Fig. 3. Comparison of temperature θ in a planar medium at different instants ζ for scattering albedo $\omega =$ (a) 0.0, (b) 0.5 and (c) 0.9.

$$\sum_{i=0}^{b} f_i^{(0)}(\vec{r},t) = \sum_{i=0}^{b} w_i T(\vec{r},t) = T(\vec{r},t) = \sum_{i=0}^{b} f_i(\vec{r},t) \tag{23}$$

To account for the volumetric radiation, Eq. (18) gets modified to [18,19]

$$f_i(\vec{r}+\vec{e}_i\Delta t, t+\Delta t) = f_i(\vec{r},t) - \frac{\Delta t}{\tau}\left[f_i(\vec{r},t) - f_i^{(0)}(\vec{r},t)\right] - \left(\frac{\Delta t}{\rho c_p}\right) w_i \nabla\cdot\vec{q}_R \tag{24}$$

Eq. (24) is the desired equation to be used in the LBM that gives the same solution as that given by the energy equation (1).

With the LBM on non-uniform lattices, lattices are not of the same size, and if the velocities are calculated based on the respective lattice sizes, all the particle distribution functions f_i will not be available for collision at the same instant which is a pre-requisite in the LBM [1–25]. To obviate this difficulty, all the particle distribution functions f_i from all the lattice centers are allowed to move with the same velocity which corresponds to the smallest size lattice. However with this, the f_i from a given lattice centre are not equidistant from the neighboring lattice centers. To allow the collision at the same instant, and thus to have a single relaxation time, the f_i in a given direction are interpolated to make them reach the neighboring lattice centers and thus remain available for collision at the same instant. This very interpolation concept has been recently used for fluid mechanics problems by Lu et al. [27], Ubertini and Succi [28] and Imamura et al. [29].

In case of a 1-D planar medium problem, in which we have used the D1Q2 lattice, linear interpolation of f_i have been done as suggested by Ubertini and Succi [28]. However, for a better accuracy, for the 2-D rectangular enclosure problem, as proposed by Lu et al. [27] quadratic interpolations in a given direction with three known points have been carried out. Further, to reduce the memory requirement and CPU times, as suggested by Lu et al. [27], interpolations of f_i have been done at the propagation step itself.

3. Results and discussion

The following two benchmark problems are considered to validate the usage of the LBM on non-uniform lattices

in solving the energy equations of transient conduction and radiation heat transfer problems.

- Initially the 1-D planar conducting and radiating participating medium is at a temperature T_E equal to that of the east boundary. Suddenly the west boundary is brought to a temperature T_W and for all times $t \geqslant 0$, it is maintained at this temperature. The boundaries of the absorbing, emitting and scattering medium are diffuse gray. Thermophysical and optical properties are considered constant.
- Initially the 2-D square enclosure is cold. Suddenly the temperature of the south boundary is raised to T_S and for all times $t \geqslant 0$ it is maintained at this temperature. The boundaries of the absorbing, emitting and scattering medium are diffuse gray. Thermophysical and optical properties are considered constant.

In both the geometries, validation of the LBM on non-uniform lattices are done for the effects of various parameters such as the extinction coefficient β, the scattering albedo ω, the conduction–radiation parameter $N\left(\frac{\kappa\beta}{4\sigma T_{ref}^3}\right)$ and the boundary emissivity ε. These validations are done for different values of lattice cluster C. In both the problems, the radiative information $\nabla \cdot \vec{q}_R$ required in solving the energy equations is computed using the FVM. The control volume of the FVM and the lattices of the LBM do not overlap (Fig. 1a and b), and thus the computed information in the two methods are not available at the same locations. In the LBM, the $\nabla \cdot \vec{q}_R$ information is required at the lattice centers. However, in the FVM, the same is available at the centers of the control volumes and centers of the control surfaces. In the 1-D case, a lattice has an overlap with two control volumes (Fig. 1a) whereas in the case of a 2-D problem, a lattice has an overlap with four control volumes (Fig. 1b). Thus to bring the $\nabla \cdot \vec{q}_R$ information to the lattice centers, averaging of $\nabla \cdot \vec{q}_R$ information known at the centers of control volumes is done. Along the corners and the boundaries, averaging is done with $\nabla \cdot \vec{q}_R$ known at the centers of the control surfaces.

It is to be further noted that in the FVM, lattice centers are situated at the centers of the control surfaces. In the LBM, the boundary lattices extend a half distance away from the boundary, however in the FVM for radiative information, control volumes are all contained within the

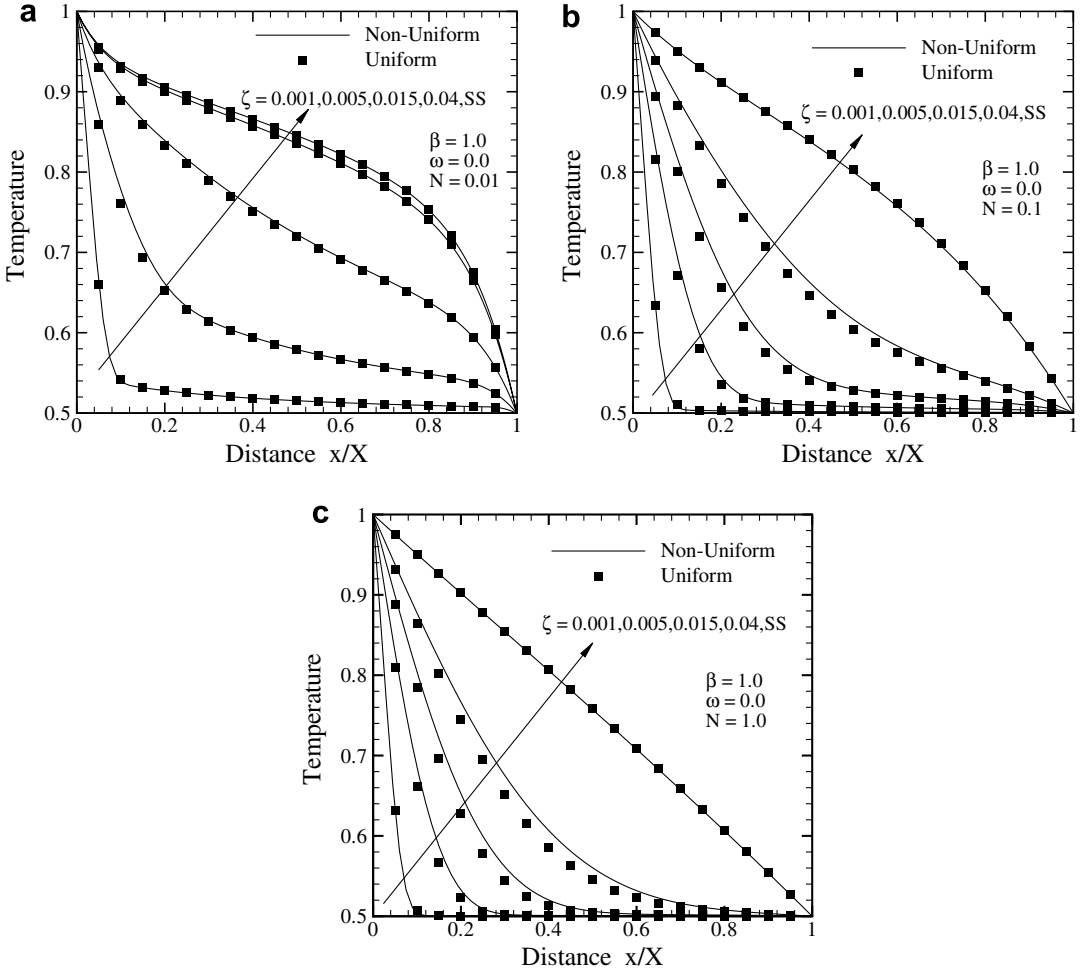

Fig. 4. Comparison of temperature θ in a planar medium at different instants ζ for conduction–radiation parameter $N =$ (a) 0.01, (b) 0.1 and (c) 1.0.

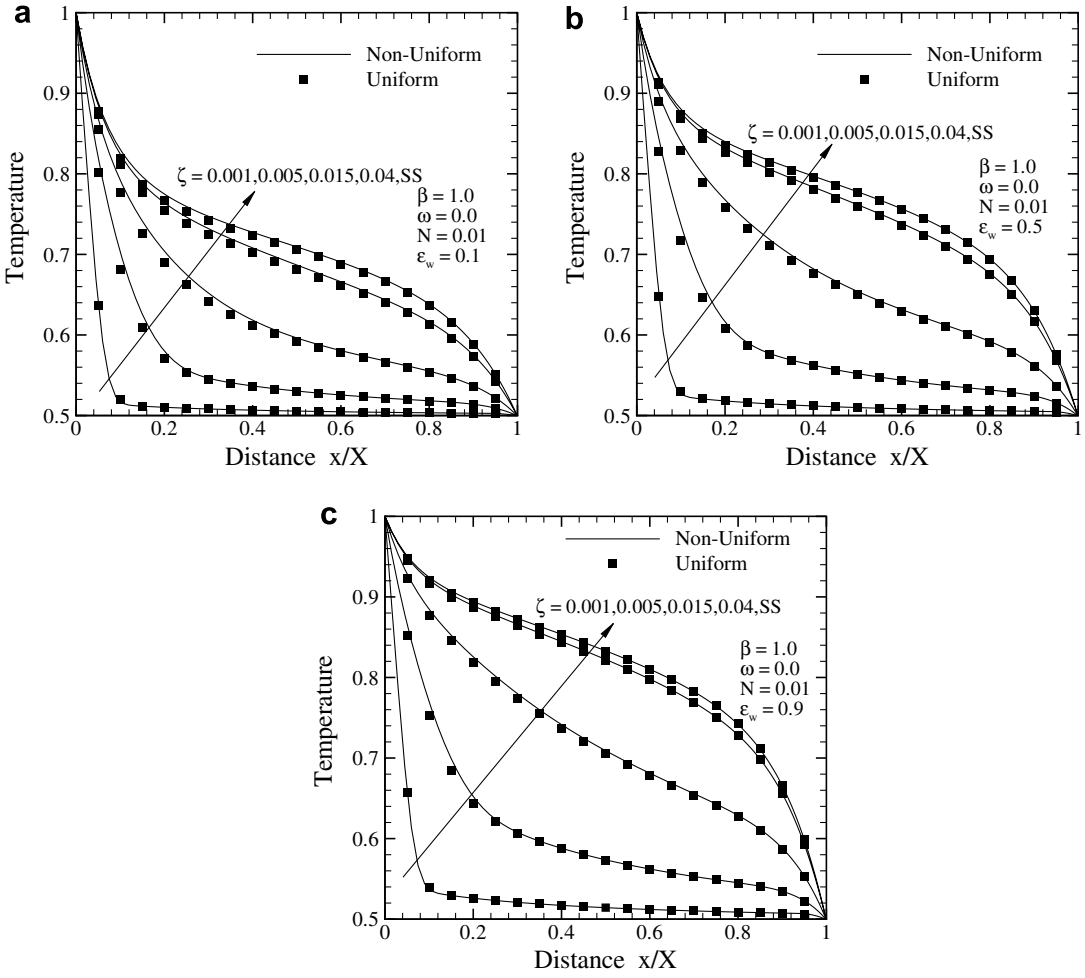

Fig. 5. Comparison of temperature θ in a planar medium at different instants ζ for emissivity of the south boundary $\varepsilon_W =$ (a) 0.1, (b) 0.5 and (c) 0.9.

boundaries (Fig. 1a and b). Thus, in every coordinate direction, the number of control volumes in the FVM is one less than the number of lattices in the LBM. Also the corner lattices and the control volumes are of the same size (Fig. 1b).

3.1. Conduction and radiation heat transfer in a 1-D planar medium

In this case, non-uniform lattices (Fig. 2) were generated using the following expression

$$x_n = \left\{ \frac{n-1}{n_{\max}} + \frac{C}{\pi} \sin\left(\frac{\pi(n-1)}{n_{\max}} \right) \right\}, \tag{25}$$

where x_n is the location of the lattice centre in the LBM, $n_{\max}$ is the total number of lattices and C is a constant ($0 \leqslant |C| \leqslant 1$) that determines clustering. For $C = 0$, uniform size lattices are obtained (Fig. 2a). For lattices/control volumes in Fig. 2b, $C = 0.5$ and that for Fig. 2c, $C = -0.5$. The type of lattices/control volumes in Fig. 2d and e are generated by dividing the solution domain in four zones and considering positive or negative values of C.

To establish the workability of the LBM–FVM with non-uniform lattices/control volumes, runs were taken for different types of clustering as shown in Fig. 2c and d. In all the cases, results of the non-uniform lattices/control volumes were compared against LBM–FVM with uniform lattices/control volumes (Fig. 2a). The number of uniform and non-uniform lattices/control volumes in the LBM–FVM was taken the same.

While generating the results, non-dimensional time step $\Delta\zeta = 1.0 \times 10^{-4}$ ($\zeta = \alpha\beta^2 t$) was considered and steady-state condition was assumed to have been achieved when the maximum variation in temperature $\theta = \frac{T}{T_W}$ at any location between two consecutive time levels did not exceed 1.0×10^{-6}. In both non-uniform and uniform lattices/control volumes, beyond 101 lattices in the LBM and 100 controls volumes and 10 directions in the FVM, no significant changes in results were observed.

It is to be noted that in case of a 1-D planar medium, radiation is azimuthally symmetric. Thus, 10 equally spaced directions in the FVM was considered by discretizing the polar angle $\theta (0 \leqslant \theta \leqslant \pi)$.

To compare results of the LBM–FVM on non-uniform lattices/control volumes with that of the LBM–FVM on

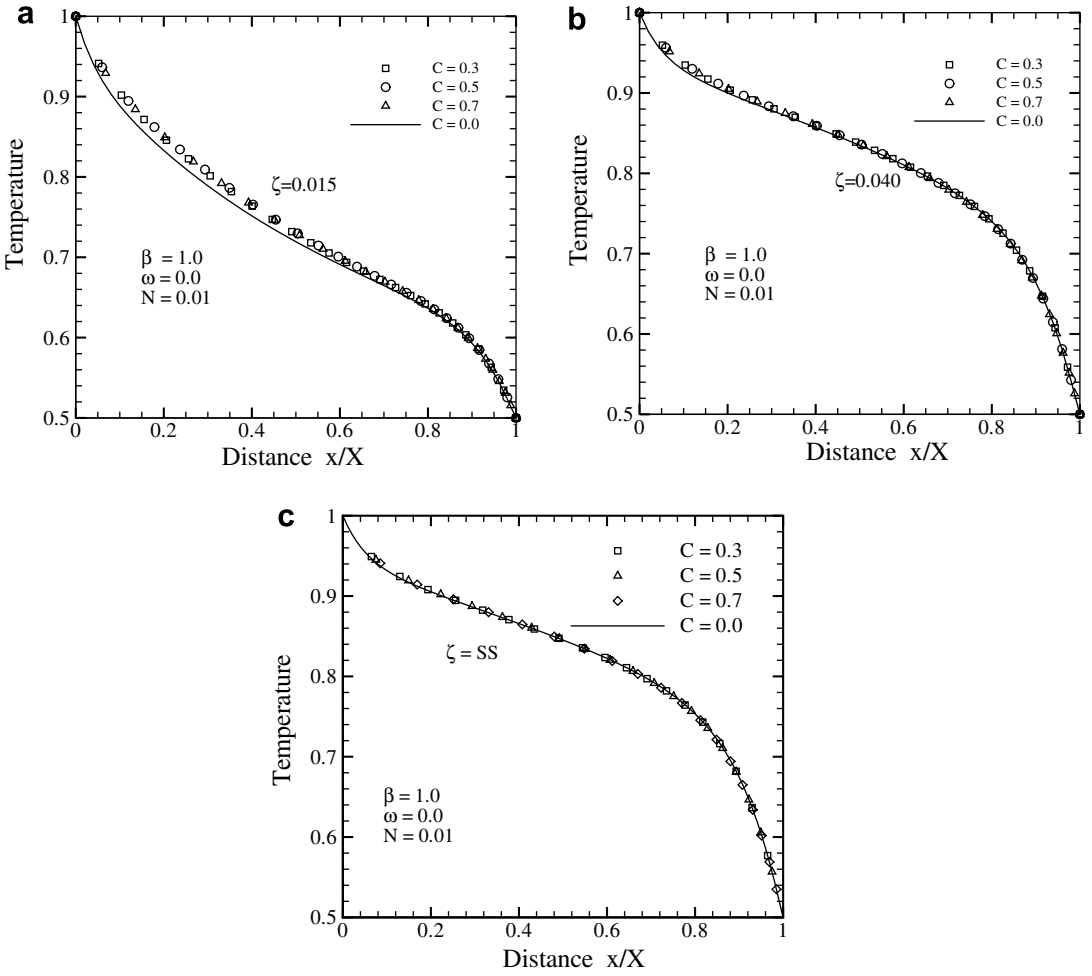

Fig. 6. Comparison of temperature θ in a planer medium for different cluster values $C = 0.0$, 0.3, 0.5 and 0.7 at time (a) $\zeta = 0.015$, (b) $\zeta = 0.040$ and (c) steady state.

uniform lattices/control volumes, in Table 1, at time $\zeta = 0.05$, temperature $\theta = \frac{T}{T_W}$ results are compared with those reported in the literature [31–34]. With clustering parameter $C = 0.5$, extinction coefficient $\beta = 1.0$, scattering albedo $\omega = 0.5$, conduction–radiation parameter $N = \frac{\kappa\beta}{4\sigma T_W^3} = 0.1$ and $T_E = 0.0$, at three locations in the medium *viz.* $x/X = 0.25$, 0.50 and 0.75, this comparison has been made for two sets of boundary emissivities ε_W and ε_E. It is observed from Table 1 that the results for the both uniform and non-uniform lattices/control volumes are in good agreements with each other and they are closely matching with those reported in the literature [31–34].

In Figs. 3–5, comparisons of temperature $\theta = \frac{T}{T_W}$ results with uniform ($C = 0.0$) lattices/control volumes have been made for non-uniform lattices/control volumes with $C = 0.5$. In Fig. 6, results have been compared for different values of C.

In Fig. 3, for extinction coefficient $\beta = 1.0$ and conduction–radiation parameter $N = 0.01$, temperature θ computed from the LBM–FVM with uniform and non-uniform lattices/control volumes have been compared for the effects of the scattering albedo ω. It can be seen from the figure that results for the both cases are matching very well. The number of iterations for the steady-state (SS) solutions in the LBM–FVM with non-uniform lattices/control volumes for $\omega = 0.0$, 0.5 and 0.9 were 869, 1144 and 2492. The same in case of the LBM–FVM with uniform lattices/control volumes were found to be 881, 1163 and 2639.

In Fig. 4, for $\omega = 0.0$ and $\beta = 1.0$, comparisons have been shown for three values of the conduction–radiation parameter N. It is seen that for both radiation dominated ($N = 0.01$) and conduction dominated ($N = 1.0$) cases, the result for the steady state condition with non-uniform lattices/control volumes match well with those with uniform lattices/control volumes. It can be seen from the figure that at all times ζ, the results with non-uniform lattices/control volume give slightly higher value with those with uniform lattices/control volumes. For non-uniform lattices/control volumes, the numbers of iterations for the steady-state results were found to be 869, 3450 and 4887 for$N = 0.01$, 0.01 and 0.1, respectively. The same for uniform lattices/control volumes were found to be 881, 3706 and 5764.

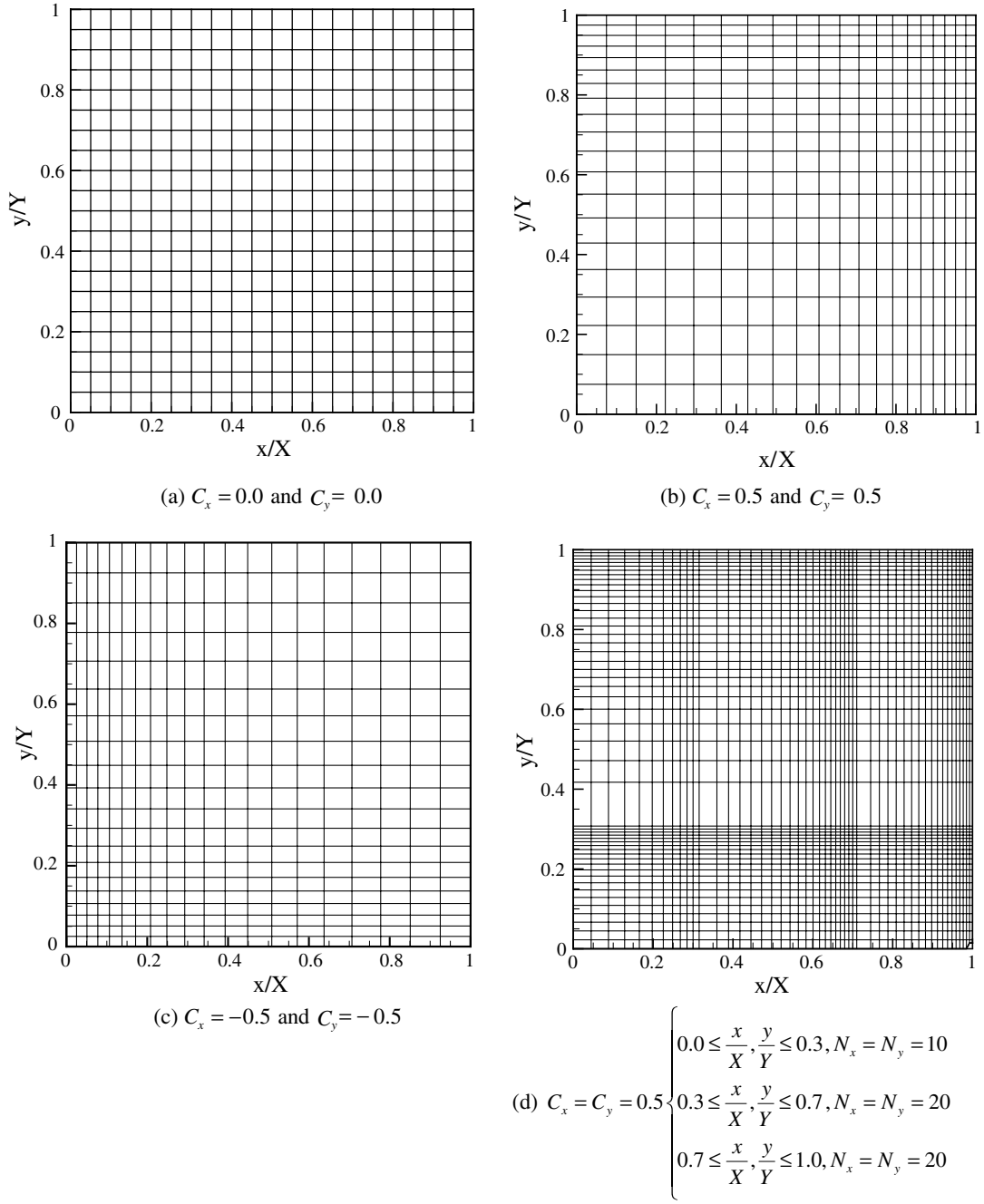

(a) $C_x = 0.0$ and $C_y = 0.0$

(b) $C_x = 0.5$ and $C_y = 0.5$

(c) $C_x = -0.5$ and $C_y = -0.5$

(d) $C_x = C_y = 0.5$ $\begin{cases} 0.0 \le \frac{x}{X}, \frac{y}{Y} \le 0.3, N_x = N_y = 10 \\ 0.3 \le \frac{x}{X}, \frac{y}{Y} \le 0.7, N_x = N_y = 20 \\ 0.7 \le \frac{x}{X}, \frac{y}{Y} \le 1.0, N_x = N_y = 20 \end{cases}$

Fig. 7. Different types of non-uniform lattices for 2-D geometry.

In Fig. 5, for $\beta = 1.0$, $\omega = 0.0$ and $N = 0.01$, with east boundary as black $\varepsilon_E = 1.0$, comparisons of the temperature results have been made for the effect of west boundary emissivity ε_W. It is seen that at all times, results with non-uniform lattices/control volumes compare very well with those of the non-uniform lattices/control volumes. In this case too, the LBM–FVM with non-uniform lattices/control volumes were found to converge fast. For $\varepsilon_W = 0.1$, 0.5 and 0.9, number of iterations with LBM–FVM with non-uniform lattices/control volumes were 1162, 995 and 892, respectively. The same for the other case were 1193, 1024 and 905.

In Fig. 6, for $\beta = 1.0$, $\omega = 0.0$, N = 0.01, $\varepsilon_W = \varepsilon_E = 1.0$, temperature θ results for different cluster values C have been compared at $\zeta = 0.015$, 0.040 and steady-state. It is seen from this figure for different clustering values, results are in good agreement with each other.

3.2. Conduction and radiation heat transfer in a 2-D square enclosure

To validate the LBM–FVM on non-uniform lattices/control volumes, next we consider transient conduc-

Table 2
Comparison of steady-state centerline ($x/X = 0.5$) temperature at three locations in a black square enclosure; $\omega = 0.0$

β	N	Centreline T/T_S at y/Y	Wu and Ou [36]	Yuen and Takara [35]	Mishra et al. [37]	Uniform lattices/control volumes	Non-uniform lattices/control volumes
0.1	0.1	0.3	0.733	0.733	0.734	0.734	0.741
		0.5	0.626	0.630	0.626	0.626	0.633
		0.7	0.561	0.563	0.561	0.561	0.566
1.0	1.0	0.3	0.733	0.737	0.737	0.737	0.734
		0.5	0.630	0.630	0.630	0.630	0.638
		0.7	0.560	0.560	0.564	0.564	0.570
1.0	0.1	0.3	0.760	0.763	0.759	0.759	0.766
		0.5	0.663	0.661	0.663	0.664	0.674
		0.7	0.590	0.589	0.594	0.596	0.604
1.0	0.01	0.3	0.791	0.807	0.789	0.784	0.784
		0.5	0.725	0.726	0.725	0.726	0.728
		0.7	0.663	0.653	0.666	0.678	0.682
5.0	0.1	0.3	0.834	0.802	0.802	0.800	0.803
		0.5	0.689	0.707	0.708	0.706	0.711
		0.7	0.585	0.626	0.628	0.625	0.631

tion and radiation heat transfer in a 2-D square enclosure (Fig. 1b). In this case, initially the entire system is at a temperature $T_0 = T_N = T_W = T_E$. For $t > 0$, the south boundary temperature is raised to $T_S = 2T_0$. The enclosed gray-homogeneous medium is absorbing, emitting and isotropically scattering.

The non-uniform size lattices/control volumes were generated from the following expressions

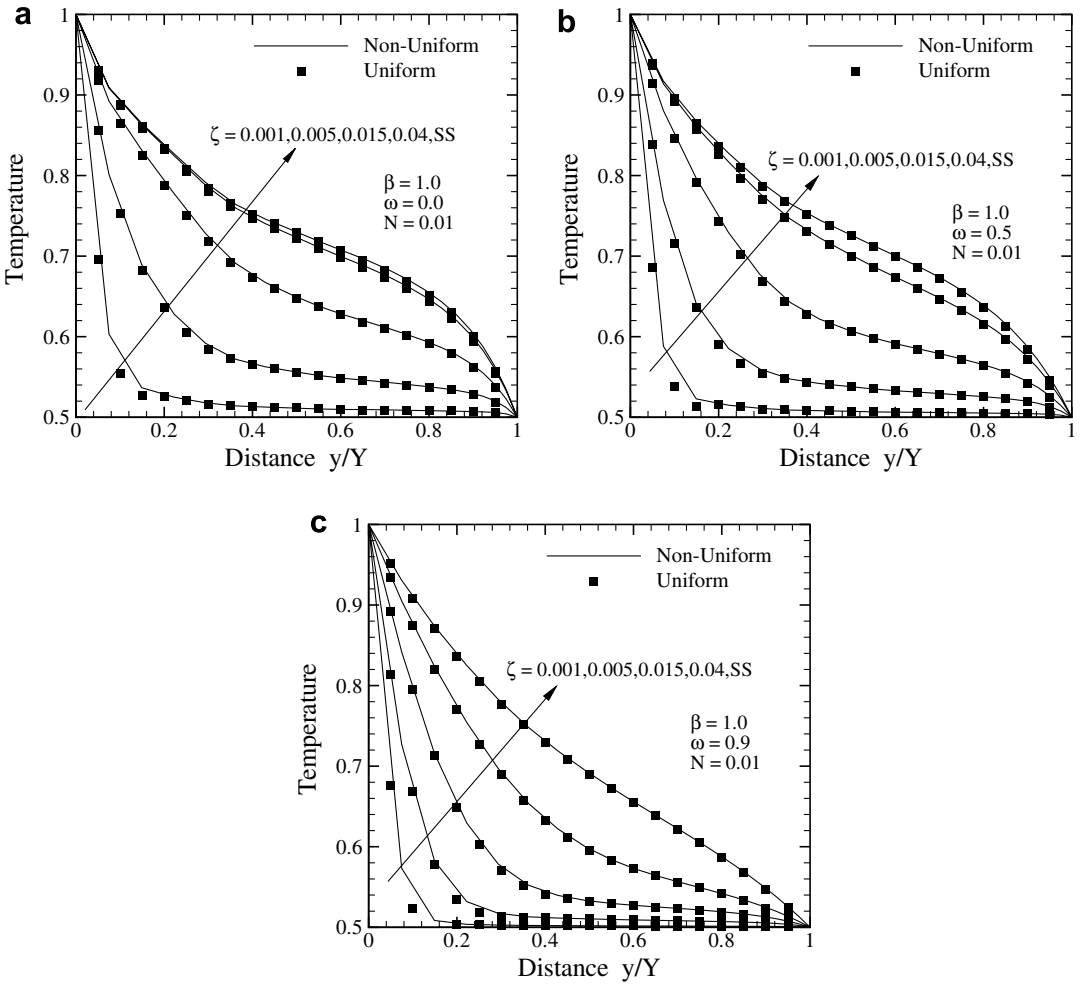

Fig. 8. Comparison of centerline temperature θ in a 2-D square enclosure at different instants ζ for scattering albedo $\omega =$ (a) 0.0, (b) 0.5 and (c) 0.9.

$$x_n = \left\{\frac{n-1}{N_x} + \frac{C_x}{\pi}\sin\left(\frac{\pi(n-1)}{N_x}\right)\right\} \quad (26)$$

$$y_n = \left\{\frac{n-1}{N_y} + \frac{C_y}{\pi}\sin\left(\frac{\pi(n-1)}{N_y}\right)\right\}, \quad (27)$$

where x_n and y_n are the location of the lattice centre in the LBM and the control volume corner in the FVM in the x and y directions, respectively. N_x and N_y are the total number of lattices/control volumes in the x and y direction, respectively and C_x $(0 \leqslant |C_x| \leqslant 1)$ and C_y $(0 \leqslant |C_y| \leqslant 1)$ are parameter that determines clustering. For the four different sets of C_x and C_y, the 2-D lattices are shown in Fig. 7a–d. With $C_x = 0$ and $C_y = 0$, uniform size lattices/control volumes are obtained (Fig. 7a). In the present work, numerical experiments were performed for the four different types of lattices shown in Fig. 7a–d.

In the 2-D case too, like the 1-D case, the non-dimensional time step $\Delta\zeta = 1.0 \times 10^{-4}$ was considered and steady-state condition was assumed to have been achieved when the maximum variation in temperature $\theta = \frac{T}{T_S}$ at any location between two consecutive time levels did not exceed 1.0×10^{-6}. No significant changes in results were observed beyond 21×21 lattices in the LBM and 20×20 control volumes and 8×8 directions over the spherical space in the FVM. The numbers of lattices/control volumes and directions were same in both LBM–FVM with uniform and non-uniform lattices/control volumes.

In Table 2, for the three values of the extinction coefficient $\beta = 0.1$, 1.0 and 5.0, and the three values of the conduction–radiation parameter $N = 0.01$, 0.1 and 1.0, with scattering albedo $\omega = 0.0$, the LBM–FVM centerline $\left(\frac{x}{X} = 0.5\right)$ non-dimensional temperature θ results at three $\frac{y}{Y}$ locations for uniform and non-uniform lattices/control volumes of the LBM–FVM are compared with those of Yuen and Takara [35], Wu and Ou [36] and Mishra et al. [37]. It can be seen that the LBM–FVM results for uniform and non-uniform lattices/control volumes are in good agreement with those available in the literature [35–37].

In the following paragraphs, centerline $\left(\frac{x}{X} = 0.5\right)$ non-dimensional temperature θ along $\frac{y}{Y}$ and for the steady state

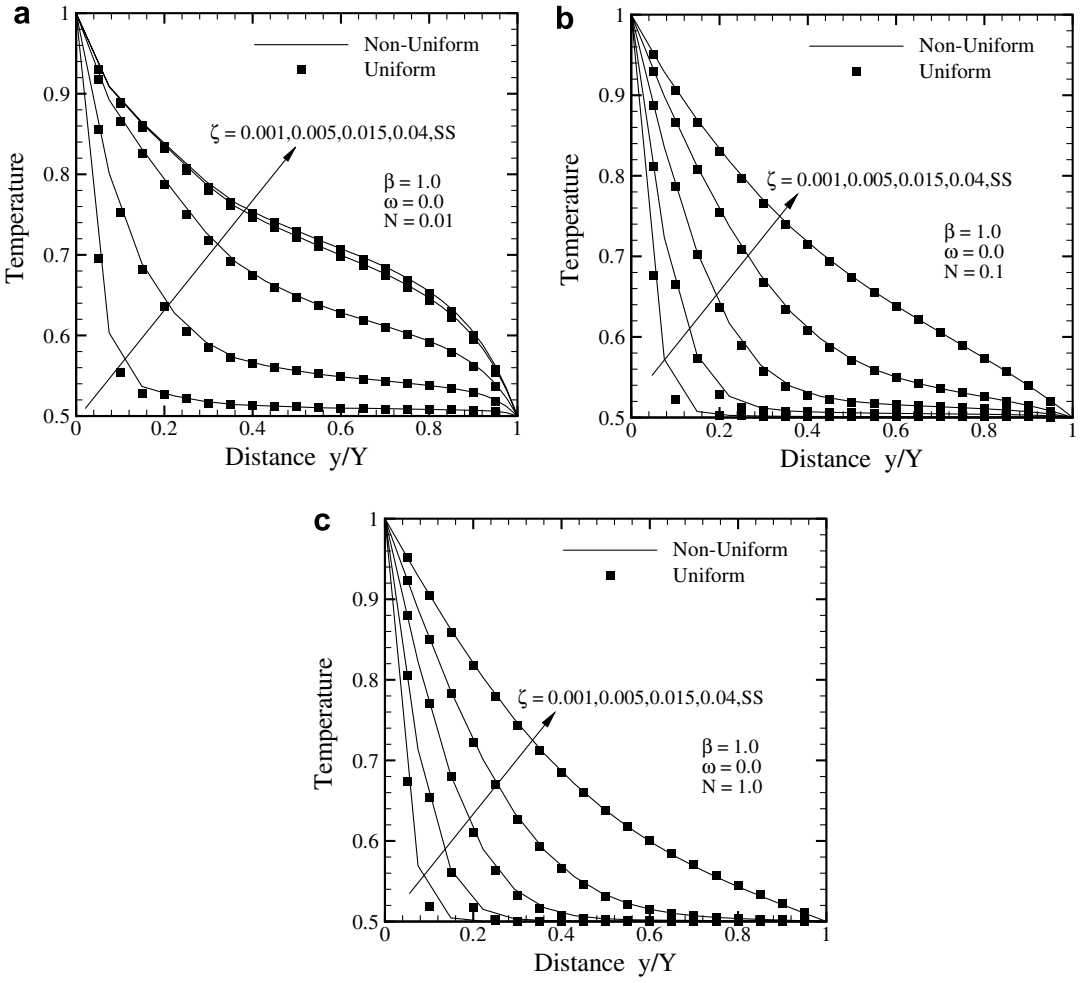

Fig. 9. Comparison of centerline temperature θ in a 2-D square enclosure at different instants ζ for conduction–radiation parameter $N =$ (a) 0.01, (b) 0.1 and (c) 1.0.

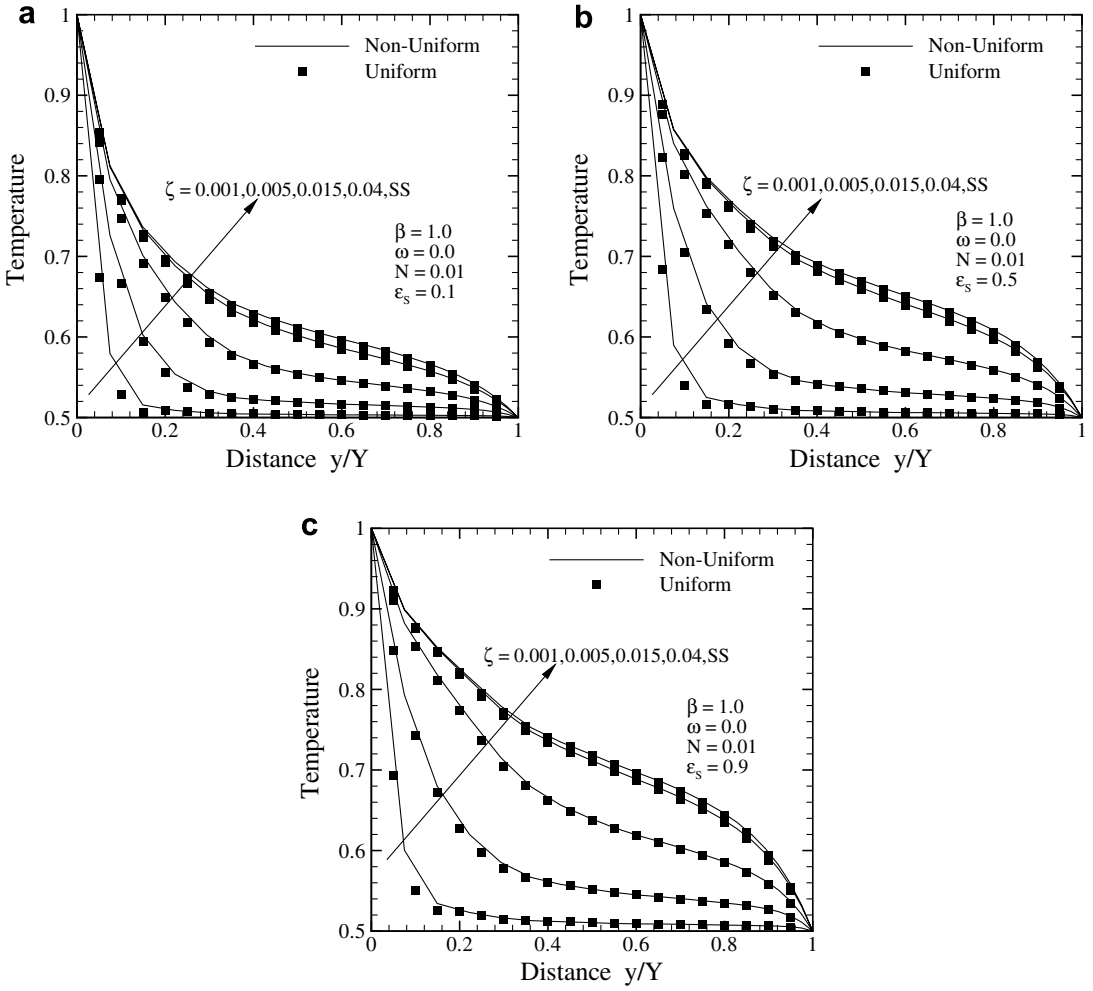

Fig. 10. Comparison of centerline temperature θ in a 2-D square enclosure at different instants ζ for (a) emissivity of the south boundary $\varepsilon_S = 0.1$, (b) 0.5 and (c) 0.9.

solutions, the numbers of iterations with uniform and non-uniform lattices/control volumes of the LBM–FVM are compared for the effects of various parameters including the clustering value.

In Fig. 8, for $\beta = 1.0$ and $N = 0.01$, temperature $\theta(T/T_S)$ computed from the LBM–FVM with uniform and non-uniform lattices/control volumes have been compared for the effects of the scattering albedo ω. It can be seen from the figure that at all times ζ, the results of the non-uniform and uniform lattices are in good agreements. The number of iterations for the steady-state solutions with non-uniform lattices/control volumes for $\omega = 0.0$, 0.5 and 0.9 were 875, 1210 and 2439. The same with uniform lattices/control volumes were found to be 872, 1204 and 2218.

In Fig. 9, for $\omega = 0.0$ and $\beta = 1.0$, comparisons of temperature θ have been shown for three values of the conduction–radiation parameter N. It is seen that for both radiation dominated ($N = 0.01$) and conduction dominated ($N = 1.0$) cases, result for the steady state condition with non-uniform lattices/control volumes match well with those with uniform lattices/control volumes. For non-uniform lattices/control volumes, the numbers of iterations for the steady-state results were found to be 875, 2788 and 3501 for $N = 0.01$, 0.01 and 0.1, respectively. The same for uniform lattices/control volumes were found to be 872, 2764 and 3469.

In Fig. 10, for $\beta = 1.0$, $\omega = 0.0$ and $N = 0.01$, comparisons of temperature θ have been made for different values of the south boundary emissivity ε_S. Other three boundaries are taken black. It is seen that at all times, results with non-uniform lattices/control volumes compare very well with those of the non-uniform lattices/control volumes. For $\varepsilon_W = 0.1$, 0.5 and 0.9, number of iterations with non-uniform lattices/control volumes were 1049, 964 and 891, respectively. The same for the uniform lattices/control volumes case were 1048, 963 and 888.

With $\beta = 1.0$, $\omega = 0.0$ and $N = 0.01$ with all four boundaries black, in Fig. 11, temperature θ results have been compared for the four sets of clustering parameter $C_x = C_y = C$. In this figure, $C = 0.0$, stands for uniform lattices/control volumes. It is observed at three time levels including the steady-state, results for all values of C are in good agreements.

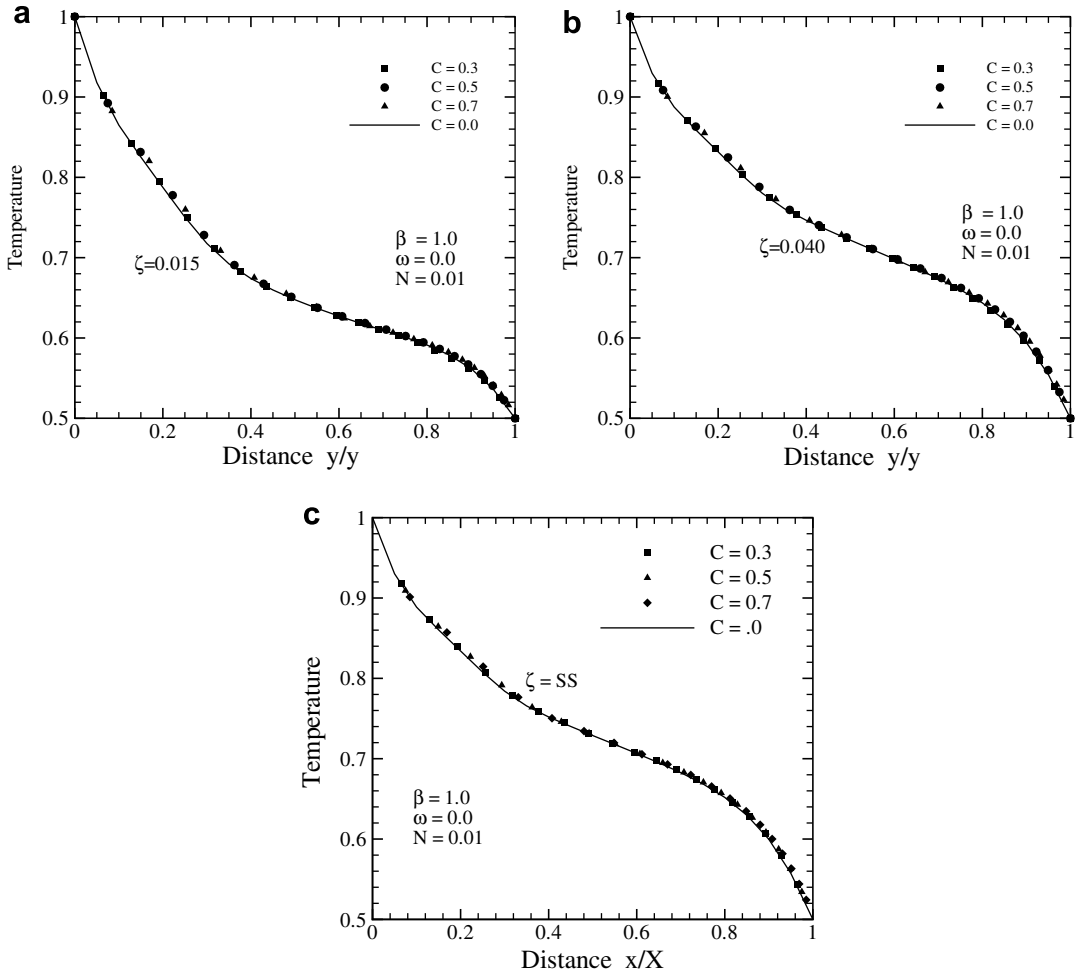

Fig. 11. Comparison of centerline temperature θ in a 2-D square enclosure at steady state for different types of lattices using quadratic interpolation scheme at non-dimensional time (a) $\zeta = 0.015$, (b) $\zeta = 0.040$ and (c) steady state.

4. Conclusions

Application of the LBM so far applied to heat transfer problems with uniform lattices was extended to non-uniform lattices. To facilitate collisions to take place at the same instant, interpolations of the particle distribution functions were done and the single relaxation time based on the smallest size lattice was used for all the lattices. To demonstrate its workability, transient conduction and radiation heat transfer problems in 1-D planar and 2-D rectangular geometries were considered. The radiative component of the energy equation was computed using the FVM and then the energy equation was solved using the LBM. Results of the LBM–FVM with uniform lattices/control volumes were first benchmarked with those reported in the literature. For various parameters including the clustering parameter, results of the uniform and non-uniform lattices/control volumes were found in good agreements. In case of a 1-D planar medium, for all the cases considered, LBM–FVM with non-uniform lattices/control volumes were found to take less number of iterations for the steady-state solutions. An opposite trend was observed in case of the 2-D geometry.

References

[1] R. Benzi, S. Succi, M. Vergassola, The lattice Boltzmann equation: theory and applications, Phys. Rep. 222 (1992) 145–197.
[2] F. Massaioli, R. Benzi, S. Succi, Exponential tails in two-dimensional Rayleigh–Bénard convection, Europhys. Lett. 21 (1993) 305–310.
[3] X. Shan, Simulation of Rayleigh–Benard convection using a lattice Boltzmann method, Phys. Rev. E 55 (1997) 2780–2788.
[4] S. Chen, G.D. Doolen, Lattice Boltzmann method for fluid flows, Annu. Rev. Fluid Mech. 30 (1998) 329–364.
[5] G.D. Fabritiis, A. Mancini, D. Mansutti, S. Succi, Mesoscopic models of liquid/solid phase transitions, Int. J. Mod. Phys. C 8 (1998) 1–11.
[6] X. He, S. Chen, G.D. Doolen, A novel thermal model for the lattice Boltzmann method in incompressible limit, J. Comput. Phys. 146 (1998) 282–300.
[7] H. Xi, G. Peng, S.-H. Chou, Finite-volume lattice Boltzmann schemes in two and three dimensions, Phys. Rev. E 60 (1999) 3380–3388.
[8] N. Takada, M. Misawa, A. Tomiyama, S. Fujiwara, Numerical simulation of two- and three-dimensional two-phase fluid motion by lattice Boltzmann method, Comput. Phys. Commun. 129 (2000) 233–236.
[9] D.A. Wolf-Gladrow, Lattice-Gas Cellular Automata and Lattice Boltzmann Models: An Introduction, Springer-Verlag, Berlin-Heidelberg, 2000.
[10] S. Succi, The Lattice Boltzmann Method for Fluid Dynamics and Beyond, Oxford University Press, 2001.

[11] W. Miller, S. Succi, D. Mansutti, Lattice Boltzmann model for anisotropic liquid–solid phase transition, Phys. Rev. Lett. (2001) 3578–3581.
[12] R.R. Nourgaliev, T.N. Dinh, T.G. Theofanous, D. Joseph, The lattice Boltzmann equation method: theoretical interpretation, numeric and implications, Int. J. Multiphas. Flow 29 (2003) 117–169.
[13] L. Zhu, D. Tretheway, L. Petzold, C. Meinhart, Simulation of fluid slip at 3-D hydrophobic micro channel walls by the lattice Boltzmann method, J. Comput. Phys. 202 (2005) 181–195.
[14] W.-S. Jiaung, J.R. Ho, C.-P. Kuo, Lattice Boltzmann method for heat conduction problem with phase change, Numer. Heat Transfer B 39 (2001) 167–187.
[15] J.R. Ho, C.-P. Kuo, W.-S. Jiaung, C.-J. Twu, Lattice Boltzmann scheme for hyperbolic heat conduction equation, Numer. Heat Transfer B 41 (2002) 591–607.
[16] J.R. Ho, C.-P. Kuo, W.S. Jiaung, Study of heat transfer in multilayered structure within the framework of dual-phase-lag heat conduction model using lattice Boltzmann method, Int. J. Heat Mass Transfer 46 (2003) 55–69.
[17] D. Chatterjee, S. Chakraborty, An enthalpy-based lattice Boltzmann model for diffusion dominated solid–liquid phase transformation, Phys. Lett. A 341 (2005) 320–330.
[18] S.C. Mishra, A. Lankadasu, Transient conduction–radiation heat transfer in participating media using the lattice Boltzmann method and the discrete transfer method, Numer. Heat Transfer A 47 (2005) 935–954.
[19] S.C. Mishra, A. Lankadasu, K. Beronov, Application of the lattice Boltzmann method for solving the energy equation of a 2-D transient conduction–radiation problem, Int. J. Heat Mass Transfer 48 (2005) 3648–3659.
[20] I. Rasin, S. Succi, W. Miller, A multi-relaxation lattice kinetic method for passive scalar diffusion, J. Comput. Phys. 206 (2005) 453–462.
[21] R. Raj, A. Prasad, P.R. Parida, S.C. Mishra, Analysis of solidification of a semitransparent planar layer using the lattice Boltzmann method and the discrete transfer method, Numer. Heat Transfer Part A 49 (2006) 279–299.
[22] P.R. Parida, R. Raj, A. Prasad, S.C. Mishra, Solidification of a semitransparent planar layer subjected to radiative and convective cooling, J. Quant. Spectrosc. Radiat. Transfer (2007), doi:10.1016/j.jqsrt.2007.02.004.
[23] N. Gupta, G.R. Chaitanya, S.C. Mishra, Lattice Boltzmann method applied to variable thermal conductivity conduction and radiation problems, J. Thermophys. Heat Transfer 20 (2006) 895–902.
[24] S.C. Mishra, H.K. Roy, Solving transient conduction–radiation problems using the lattice Boltzmann method and the finite volume method, J. Comput. Phys. 223 (2007) 89–107.
[25] B. Mondal, S.C. Mishra, Application of the lattice Boltzmann method and discrete ordinate method for solving transient conduction and radiation heat transfer problems, Numer. Heat Transfer Part A, in press.
[26] F. Nannelli, S. Succi, The lattice Boltzmann equation on irregular lattices, J. Stat. Phys. 68 (1992) 401–407.
[27] Z. Lu, Y. Liao, D. Qian, J.B. McLaughlin, J.J. Derksen, K. Kontomaris, Large eddy simulations of a stirred tank using the lattice Boltzmann method on a non-uniform grid, J. Comput. Phys. 181 (2002) 675–704.
[28] S. Ubertini, S. Succi, Recent advances of Lattice Boltzmann techniques on unstructured grids, Pros. Comput. Fluid Dyn. 5 (2005) 85–96.
[29] T. Imamura, K. Suzuki, T. Nakamura, M. Yoshida, Acceleration of steady-state lattice Boltzmann simulations on non-uniform mesh using local time step method, J. Comput. Phys. 202 (2005) 645–663.
[30] J.C. Chai, S.V. Patankar, Finite volume method for radiation heat transfer, Adv. Numer. Heat Transfer 2 (2000) 110–135.
[31] C. Barker, W.H. Sutton, The transient radiation and conduction heat transfer in a gray participating medium with semi-transparent boundaries, radiation heat transfer, ASME J. Radiat. Heat Transfer 49 (1985) 25–36.
[32] W.H. Sutton, A short time solution for coupled conduction and radiation in a participating slab geometry, J. Heat Transfer 108 (1986) 465–466.
[33] J.H. Tsai, J.D. Lin, Transient combined conduction and radiation with anisotropic scattering, J. Thermophys. Heat Transfer 4 (1990) 92–97.
[34] P. Talukdar, S.C. Mishra, Analysis of conduction and radiation heat transfer with heat generation in participating medium using the collapsed dimension method, Numer. Heat Transfer A 39 (2001) 79–100.
[35] W.W. Yuen, E.E. Takara, Analysis of combined conductive-radiative heat transfer in a two-dimensional rectangular enclosure with a gray medium, J. Heat Transfer 110 (1988) 468–474.
[36] C.Y. Wu, N.R. Ou, Transient two-dimensional radiative and conductive heat transfer in a scattering medium, Int. J. Heat Mass Transfer 37 (1994) 2675–2686.
[37] S.C. Mishra, P. Talukdar, D. Trimis, F. Durst, Computational efficiency improvements of the radiative transfer problems with or without conduction – a comparison of the collapsed dimension method and the discrete transfer method, Int. J. Heat Mass Transfer 46 (2003) 3083–3095.